Phase diagram and spectral properties of a new exactly integrable spin-1 quantum chain

2010 J. Phys. A: Math. Theor. 43 155002

(http://iopscience.iop.org/1751-8121/43/15/155002)

J. Phys. A: Math. Theor. **43** (2010) 155002 (15pp) doi:10.1088/1751-8113/43/15/155002

Phase diagram and spectral properties of a new exactly integrable spin-1 quantum chain

Francisco C Alcaraz and Gilberto M Nakamura

Instituto de Física de São Carlos, Universidade de São Paulo, CP 369, 13560-970, São Carlos, São Paulo, Brazil

E-mail: alcaraz@if.sc.usp.br

Received 25 August 2009, in final form 25 February 2010
Published 25 March 2010
Online at stacks.iop.org/JPhysA/43/155002

Abstract

The spectral properties and phase diagram of the exactly integrable spin-1 quantum chain introduced by Alcaraz and Bariev are presented. The model has a $U(1)$ symmetry and its integrability is associated with an unknown R-matrix whose dependence on the spectral parameters is not of a different form. The associated Bethe ansatz equations that fix the eigenspectra are distinct from those associated with other known integrable spin models. The model has a free parameter t_p. We show that at the special point $t_p = 1$, the model acquires an extra $U(1)$ symmetry and reduces to the deformed $SU(3)$ Perk–Schultz model at a special value of its anisotropy $q = \exp(\mathrm{i}2\pi/3)$ and in the presence of an external magnetic field. Our analysis is carried out either by solving the associated Bethe ansatz equations or by direct diagonalization of the quantum Hamiltonian for small lattice sizes. The phase diagram is calculated by exploring the consequences of conformal invariance on the finite-size corrections of the Hamiltonian eigenspectrum. The model exhibits a critical phase ruled by the $c = 1$ conformal field theory separated from a massive phase by first-order phase transitions.

PACS numbers: 75.10.Pq, 02.30.Ik, 05.50.+q, 05.30.−d

(Some figures in this article are in colour only in the electronic version)

1. Introduction

The anisotropic spin-1/2 Heisenberg model, or XXZ quantum chain, and the 6-vertex model are considered as paradigm of exact integrability in statistical mechanics [1]. In the XXZ quantum chain the z-component of the total magnetization is a good quantum number ($U(1)$ symmetry). Its simplest integrable generalizations that keep the $U(1)$ symmetry are spin-1 quantum chains. Models on this class are the Fateev–Zamolodchikov model [2], the Izergin–Korepin model [3], the supersymmetric $OSP(1/2)$ model [4] and the biquadratic model [5].

The integrability of these models is a consequence of the existence of a known associated R-matrix satisfying the Yang–Baxter equation. The associated R-matrix for these models are regular, i.e. depends only on the difference of the spectral parameters.

A new exactly integrable spin-1 quantum chain was derived by using the coordinate Bethe ansatz [6] or a matrix product ansatz [7]. The derivation of the integrable model through these last approaches does not depend on the knowledge of the associated R-matrix. Distinct from the other integrable [2–5] and nonintegrable [8] spin-1 models, whose physical properties are well studied, almost no physical information is known for this new quantum chain, besides its exact integrability. The unknown associated R-matrix is not regular [6] since it does not satisfy the Reshetikihin criterion [9]. The Bethe ansatz equations (BAE) that fix the eigenenergies are also quite distinct from the corresponding equations of other spin-1 integrable quantum chains.

In this paper we are going to present an extensive analytical and numerical analysis of the eigenspectra properties of this new spin-1 quantum chain. Based on solutions of the associated BAE, whenever it is possible, and diagonalizations of the quantum Hamiltonian on small lattices ($L = 2$–24), we are able to predict some of its critical properties.

The paper is organized as follows. In section 2 we present the model and the BAE that fix the eigenspectra. The model has a $U(1)$ symmetry and is exactly integrable for any value of a free parameter t_p. We show that for the special value $t_p = 1$, the model is related to the deformed $SU(3)$ Perk–Schultz model with the deformation parameter $q = \exp(\mathrm{i}2\pi/3)$ [10] in the presence of an external magnetic field. In section 3 we analyze the eigenspectra of the quantum chain in several regions with distinct values of the free parameter t_p. Based on conformal invariance predictions, the critical properties of the model are calculated. Finally in section 4 we summarize our results and present our conclusions.

2. The model

Instead of presenting the quantum Hamiltonian in terms of spin-1 $SU(2)$ matrices (S^x, S^y, S^z), it is more convenient to present it in terms of the 3×3 Weyl matrices $E^{l,m}$ $(l, m = 0, 1, 2)$, with elements $E^{l,m})_{i,j} = \delta_{l,i}\delta_{m,j}$. At each lattice site i we may have a zero particle ($n_i = 0$), one particle ($n_i = 1$) or two particles ($n_i = 2$) or equivalently $S_i^z = -1$, $S_i^z = 0$ and $S_i^z = 1$, respectively. The dynamics of these particles, in a periodic chain with L sites, is described by the Hamiltonian

$$H(t_p, h) = -\sum_{j=1}^{L} \sum_{\alpha,\beta,\gamma,\mu=0}^{2} \Gamma_{\gamma,\mu}^{\alpha,\beta} E_j^{\gamma,\alpha} E_{j+1}^{\mu,\beta} - h \sum_{j=1}^{L} \sum_{\alpha=1}^{2} \alpha E_j^{\alpha,\alpha}, \tag{1}$$

where

$$\begin{aligned} &\Gamma_{0,1}^{1,0} = \Gamma_{1,0}^{0,1} = \Gamma_{1,2}^{2,1} = \Gamma_{2,1}^{1,2} = -1, && \Gamma_{2,0}^{0,2} = \Gamma_{0,2}^{2,0} = -t_p, \\ &\Gamma_{0,2}^{1,1} = \Gamma_{1,1}^{0,2} = \mathrm{e}^{-\mathrm{i}\pi/3}\sqrt{t_p^2 - 1}, && \Gamma_{2,0}^{1,1} = \Gamma_{1,1}^{2,0} = -\mathrm{e}^{\mathrm{i}\pi/3}\sqrt{t_p^2 - 1} \end{aligned} \tag{2}$$

are the hopping parameters (off diagonal) and the static terms (diagonal) are given by

$$\begin{aligned} &\Gamma_{0,0}^{0,0} = \Gamma_{2,2}^{2,2} = 0, && \Gamma_{1,0}^{1,0} = \Gamma_{0,1}^{0,1} = \frac{1}{4t_p}, \\ &\Gamma_{1,1}^{1,1} = t_p + \frac{1}{2t_p}, && \Gamma_{0,2}^{0,2} = \Gamma_{2,0}^{2,0} = -\frac{t_p}{2}, \\ &\Gamma_{1,2}^{1,2} = \frac{1}{4t_p} + \mathrm{i}\frac{\sqrt{3}}{2}t_p, && \Gamma_{2,1}^{2,1} = \frac{1}{4t_p} - \mathrm{i}\frac{\sqrt{3}}{2}t_p. \end{aligned} \tag{3}$$

The parameter t_p is free and h plays the role of a magnetic field in the z-direction (z-magnetic field) or a chemical potential controlling the magnetization or the number of particles in the ground state, respectively.

The Hamiltonian (1) is non-Hermitian. It is interesting to observe that its non-Hermiticity is not only due to the presence of complex matrix elements in the diagonal (see (3)) (as occurs in the quantum deformed $SU_q(N)$ models) but also due to the presence of complex nondiagonal elements (see (2)). The Hamiltonian (1) has a $U(1)$ symmetry due to its commutation with the total density ρ of particles

$$\rho = \frac{n}{L}, \qquad n = \sum_{j=1}^{L} n_j, \qquad n_j = S_j^z + 1 = \sum_{\alpha=1}^{2} \alpha E_j^{\alpha,\alpha}. \tag{4}$$

As a consequence its associated eigenvector space can be separated into disjoint sectors labeled by the the total number of particles n (or density ρ) or equivalently by its magnetization.

The quantum chain (1) corresponds to one of the exactly integrable models introduced in [6][1]. It is given by the choice $\epsilon = 1$ in equation (15) of [6]. As compared with the original presentation of the model, we also added a harmless z-magnetic field so that the ground state of (1) at $h = 0$ has, for any value of t_p, a total density $\rho = 1$ or equivalently zero magnetization. The Hamiltonian (1) is exactly integrable for arbitrary values of the parameter t_p and magnetic field h.

At $t_p = 1$ the non-diagonal couplings $\Gamma_{2,0}^{1,1} = \Gamma_{1,1}^{2,0} = \Gamma_{0,2}^{1,1} = \Gamma_{1,1}^{0,2} = 0$ and the model has an additional $U(1)$ symmetry. The number of sites with single and double occupancy are now conserved separately. The parameter t_p can be interpreted as an anisotropy parameter, $t_p = 1$ being the isotropic point. At this isotropic point, apart from a contribution $\mathrm{i}\frac{\sqrt{3}}{2}\sum_{i=1}^{L}\left(E_i^{0,0} - E_{i+1}^{0,0}\right)$ that vanishes in the periodic chain, the Hamiltonian, with $h = 0$, is given by

$$H(t_p = 1, h = 0) = H_{PS}\left(\mathrm{i}\frac{2\pi}{3}\right) - \frac{3}{2}\sum_{j=1}^{L} E_j^{1,1} + \frac{L}{2}, \tag{5}$$

where

$$H_{PS}(\gamma) = \sum_{j=1}^{L}\sum_{\alpha=0}^{2}\Bigg\{\cosh\gamma\, E_i^{\alpha,\alpha}E_{i+1}^{\alpha,\alpha} + \sum_{\beta=\alpha+1}^{2}\left[\sinh\gamma\left(E_i^{\beta,\beta}E_{i+1}^{\alpha,\alpha} - E_i^{\alpha,\alpha}E_{i+1}^{\beta,\beta}\right) + E_i^{\alpha,\beta}E_{i+1}^{\beta,\alpha} + E_i^{\beta,\alpha}E_{i+1}^{\alpha,\beta}\right]\Bigg\} \tag{6}$$

is the deformed spin-1 $SU(3)$ Perk–Schultz model [10] at the special value of the deformation parameter $q = \mathrm{e}^{\gamma}$, $\gamma = \mathrm{i}2\pi/3$. This model is also known as the anisotropic $SU(3)$ Sutherland model [11]. It is important to stress that the related Perk–Schultz Hamiltonian is the ferromagnetic one (signal +) in the presence of a special magnetic field (value $h^1 = 3/2$, $h^2 = 0$) favoring single occupied sites. A simple calculation shows us that the ground state for the related Perk–Schultz model occurs in the sector with total density $\rho = 1$. It corresponds to the trivial state $|11\cdots1\rangle$ where all the sites are single occupied. The model (1), for $t_p \neq 1$, can then be considered as the spin-1 anisotropic Perk–Schultz model at $q = \mathrm{e}^{\mathrm{i}2\pi/3}$

[1] There is a misprint in equations (1) and (15) [6]. We should have in (1) $u E_j^{22}E_{j+1}^{00}$ the term $u(E_j^{22}E_{j+1}^{00} + E_j^{00}E_{j+1}^{22})/2$ and in equation (15) $u = \epsilon t_p + (2-\epsilon)t_p^{-1}$.

with an additional parameter that breaks partially its symmetry. For arbitrary values of t_p, the eigenenergies and momentum are given by [6]

$$E = -n\left(\frac{1}{2t_p} + h\right) + 2\sum_{j=1}^{n} \cos k_j, \qquad P = \sum_{j=1}^{n} k_j, \tag{7}$$

where $\{k_j = k(\lambda_j);\ j = 1, \ldots, n\}$ are the roots obtained from the BAE

$$e^{ik_j L} = -\prod_{l=1}^{n} \frac{\sinh(\lambda_j - \lambda_l - i2\pi/3)}{\sinh(\lambda_j - \lambda_l + i2\pi/3)}, \qquad j = 1, \ldots, n, \tag{8}$$

with

$$e^{ik_j} = \frac{\sinh\lambda_j - i\sqrt{3t_p^2 + \left(4t_p^2 - 1\right)\sinh^2\lambda_j}}{t_p(\sinh\lambda_j + i\sqrt{3}\cosh\lambda_j)}. \tag{9}$$

As we see from (9), the left-hand side of the BAE (8) is quite distinct from the corresponding equations for other exactly integrable quantum chains. In order to consider the bulk limit ($L \to \infty$), it is then necessary to study these equations for small lattice sizes. These studies, as we are going to see in the next section, will give us educated guesses for the topology of the roots $\{\lambda_j\}$ related to the low-lying eigenvalues.

Before closing this section it is interesting to consider the BAE (8)–(9) at $t_p = 1$. In this case they are given by

$$\left[\frac{\sinh(\lambda_j - i\pi/3)}{\sinh(\lambda_j + i\pi/3)}\right]^L = -\prod_{l=1}^{n} \frac{\sinh(\lambda_j - \lambda_l - i2\pi/3)}{\sinh(\lambda_j - \lambda_l + i2\pi/3)}, \qquad j = 1, \ldots, n. \tag{10}$$

These equations coincide with the BAE of the XXZ chain [1] at the special value of its anisotropy $\Delta = -(q + 1/q) = 1/2$ ($q = e^{i2\pi/3}$). However, in the XXZ chain, the density of particles is restricted to $0 \leqslant \rho \leqslant 1$ while in the model (1) $0 \leqslant \rho \leqslant 2$. Although the completeness of the Bethe ansatz solutions is always a complicated problem, we expect that at $t_p = 1$ the solution obtained from (10) is not complete. Due to the additional symmetry (conservation of the number of pairs of particles) we should start again the Bethe ansatz [6] or the matrix product ansatz [7] taking into account this new symmetry. In this case we obtain the nested BAE of the deformed $SU(3)$ Perk–Schultz model with the deformation parameter value $q = e^{i2\pi/3}$. At this point this last model is special. In [12] several conjectures about the eigenspectra of this model on its antiferromagnetic regime were made. As is well known, the eigenspectra of the anisotropic $SU(3)$ Perk–Schultz model contain all the eigenvalues of the XXZ quantum chain with the same anisotropy. The equivalence (5) then indicates that the whole eigenspectra of the XXZ with anisotropy $\Delta = 1/2$ are contained in the eigenspectra of the Hamiltonian (1) at $t_p = 1$. Moreover, a direct diagonalization of (1), with $t_p = 1$ and $h = 0$, shows that for small even lattice sizes ($L \leqslant 12$) the low-lying eigenvectors, for densities $\rho < 1$, coincide with those of the XXZ chain at the anisotropy $\Delta = 1/2$. This means that there is no double occupancy of particles on these eigenstates. This can be understood from (5) due to the presence of the magnetic field favoring single occupied sites.

3. Eigenspectra calculations

In this paper we restrict ourselves to the cases where the parameter t_p is real and positive. The eigenvalues of $H(t_p, h)$ are the same as those of $-H(-t_p, -h)$. The Hamiltonian (1) although having a real trace is non-Hermitian. The exact eigenspectra calculations for lattice

sizes $L \leqslant 12$ show that most of the eigenenergies are real. All the low-lying eigenvalues are real numbers. Imaginary eigenvalues, appearing in complex-conjugate pairs, occur only for high excited states in the eigenspectrum. We also verify that when $h = 0$ the ground state of (1) belongs, for general values of t_p, to the sector with density $\rho = 1$. Moreover, for $h = 0$, the low-lying excited states in the sectors with densities $\rho = 1 + \frac{m}{L}$ and $\rho = 1 - \frac{m}{L}$ $(m = 1, 2, \ldots)$ are degenerated. This degeneracy is not valid for higher excited states since the model (1) at $h = 0$ does not have the symmetry under the conjugation of particles: $0 \leftrightarrow 2$, $1 \leftrightarrow 1$.

At $t_p = 1$, where the model (1) recovers the deformed $SU_q(3)$ Perk–Schultz model at $q = e^{i2\pi/3}$ (see (6)), the model is massive (nonzero gap). Our numerical results indicate the same massive behavior for all values of $t_p \geqslant 0$ as long as $h = 0$. As h decreases (negative values), it reaches the critical field $h_c(t_p)$. For $h \leqslant h_c(t_p)$ the ground-state changes continuously its density of particles $\rho = \rho(h) < 1$. We do expect, in the plane (t_p, ρ), a phase diagram with massless (critical) behavior for $\rho < 1$. In this critical regime, the long-distance fluctuations should be ruled by an underlying conformal invariant field theory. The conformal central charge c of the continuum theory can be estimated from the finite-size corrections of the ground-state energy $E_0(L, t_p, \rho)$ of the finite-size L chain [13], i.e.

$$\frac{E_0(L, t_p, \rho)}{L} = e_\infty - \frac{\pi v_s c}{L^2} + o(L^{-2}), \tag{11}$$

where e_∞ is the bulk limit of the ground-state energy per site and $v_s = v_s(t_p, \rho)$ is the sound velocity that can be inferred from the energy–momentum dispersion relations. Moreover, for each primary operator $\Phi_{\Delta,\bar{\Delta}}$, with dimension $x_\Phi = \Delta + \bar{\Delta}$ and spin $s_\Phi = \Delta - \bar{\Delta}$ in the operator algebra of the underlying conformal theory, there exists an infinite tower of eigenstates whose energies $E^\Phi_{m,m'}(L)$ and momentum $P^\Phi_{m,m'}$ behave asymptotically as [14]

$$\begin{aligned} E^\Phi_{m,m'}(L) &= E_0(L) + \frac{2\pi}{L} v_s (x_\Phi + m + m') + o(L^{-1}), \\ P^\Phi_{m,m'} &= \frac{2\pi}{L}(s_\Phi + m - m'), \end{aligned} \tag{12}$$

with $m, m' = 0, 1, 2, \ldots$.

Our spectral analysis of the Hamiltonian (1) was done by solving numerically the BAE (8)–(9) using a Newton-type method, whenever it was possible. Since there is no numerical method that warranties the solution for the nonlinear equation (8), the success in finding the solutions depends very much on the ability to provide educated guesses for the approximated values. In the cases where we were not able to obtain the solutions of the BAE, our analyses were based on direct numerical diagonalizations, or by using approximated methods like the power method. On these last cases our analyses were limited for lattice sizes up to $L = 24$ sites.

According to the different topologies of roots of the BAE (8)–(9) we divide the plane (t_p, ρ) into five regions (see figure 1).

In general, the roots $\{\lambda_j\}$ of (8) are complex numbers. The numerical analysis, based on direct solutions of (8), as compared with brute force diagonalizations of the quantum chains shows that in regions 1 and 2 (see figure 1) the roots $\{\lambda_j\}$ corresponding to the low-lying eigenvalues are all real numbers. For these cases, the right-hand side of (8) is unimodular. The roots are then constrained (or not) on a finite real interval, depending on the values of t_p. If $t_p < 1/2$ (region 1) the real roots are constrained on the interval

$$-\Omega(t_p) < \lambda_j < \Omega(t_p), \tag{13}$$

where

$$\Omega(t_p) = \frac{1}{2} \cosh^{-1}\left(\frac{2t_p^2 + 1}{1 - 4t_p^2}\right). \tag{14}$$

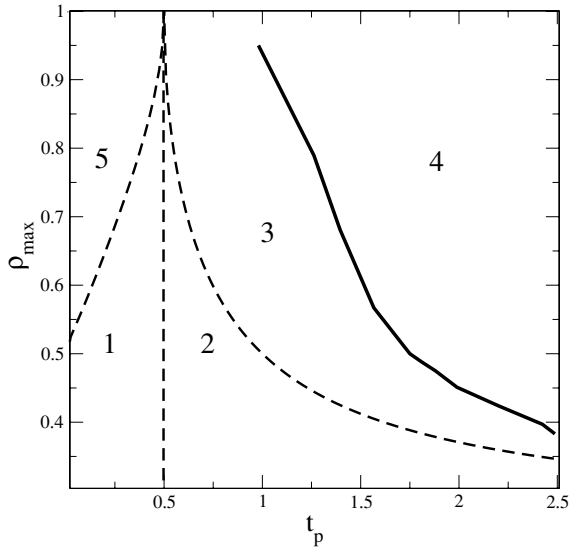

Figure 1. Phase diagram of the quantum Hamiltonian (1)–(3). In regions 1 and 2 the ground state is described by real roots of the BAE. In the other regions the ground state, besides real roots, also contains complex ones. Regions 1, 2, 3 and 5 are critical and governed by the $c = 1$ Coulomb gas conformal field theory. Region 4 is characterized by several crossing of the eigenenergies producing an oscillatory behavior in the finite energy gaps and momentum. The lines separating regions 1 and 5 and regions 2 and 3 are obtained by solving (19)–(21) and (23). A schematic line (heavy line) where we expect a first-order phase transition, separating regions 3 and 4, is also shown.

For $t_p \geqslant 1/2$ (region 2) these roots are unconstrained. For these real roots the BAE (8)–(9) take the simple from

$$Lk(\lambda_j) = 2\pi Q_j^{(n)} + \sum_{k=1}^{n} \phi(\lambda_j, -\lambda_k), \qquad j = 1, \ldots, n, \tag{15}$$

where

$$k(\lambda) = \theta_2(\lambda) - \theta_1(\lambda), \quad \phi(\lambda) = 2\arctan\left(\frac{\tanh\lambda}{\sqrt{3}}\right),$$
$$\theta_2(\lambda) = -\arctan\left(\frac{\sqrt{3t_p^2 + \left(4t_p^2 - 1\right)\sinh^2\lambda}}{\sinh\lambda}\right), \tag{16}$$
$$\theta_1(\lambda) = \arctan(\sqrt{3}\coth\lambda),$$

and $Q_j^{(n)} (j = 1, \ldots, n)$ are integers or odd-half integers, depending on the particular eigenstate. As before, the eigenenergies and momenta are given by (7).

In order to illustrate we present in table 1 some eigenenergies obtained by solving the BAE (15) in region 1. We take in (1) the magnetic field $h = 0$. They are obtained for several lattice sizes L at $t_p = 0.2$, 0.3 and 0.4 and densities $\rho = 0.6$, 0.65 and 0.7, respectively.

They are zero (mod. π) momentum eigenstates with roots $\{\lambda_j\}$ symmetrically distributed around the origin. The corresponding quantum numbers in (16) are $Q_j^{(n)} = \pm\left(-\frac{L}{2} + j\right)$ $(j = 1, \ldots, n = \rho L)$. The finite-size corrections of the ground-state energies indicate that in regions 1 and 2 the Hamiltonian (1) is critical and conformally invariant. Relation (11) gives us an estimate for the conformal anomaly c of the underlying conformal field theory. In

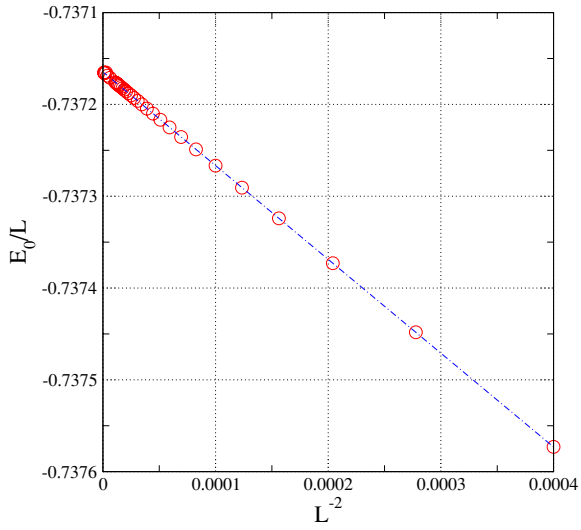

Figure 2. Ground-state energy per site of the Hamiltonian (1) as a function of $1/L^2$ for $t_p = 0.2$, $\rho = 0.6$. We set $h = 0$ in the figure. This point belongs to region 1 in figure 1.

Table 1. Lowest eigenenergies per site of the Hamiltonian (1) with $h = 0$ for some values of L, t_p and density of particles ρ. These points belong to region 1 (see figure 1). They are obtained by solving directly the BAE (15). They last line is the asymptotic value obtained from the solution of (19)–(22).

$L\backslash(t_p, \rho)$	(0.2, 0.6)	(0.3, 0.65)	(0.4, 0.7)
10	−2.247 455 86	–	−1.705 796 04
100	−2.237 266 00	−1.865 550 23	−1.699 909 39
200	−2.237 190 21	−1.865 484 82	−1.696 538 25
1000	−2.237 165 69	−1.865 470 50	−1.696 515 39
Ext.	−2.237 164 39	−1.865 465 61	−1.696 240 38

figure 2 we show, as an example, the ground-state energy per site as a function of $1/L^2$ for the quantum chain with $t_p = 0.2$, density $\rho = 0.6$ and $h = 0$. We clearly see a linear behavior as predicted by conformal invariance (see (11)). The linear coefficient of the dot line in figure 2 gives us, from (11), an estimate for the product $2\pi v_s c$. The sound velocity v_s is more difficult to estimate from numerical solutions of (15)–(16), since it demands the calculation of excited states with nonzero momenta. The BAE roots in this case are not symmetric. A possible way to circumvent this problem is to seek for excited zero momentum states related to higher values of $m = m'$ in the conformal tower (12) of the identity operator ($x_\phi = 0$). Our numerical analysis indicates that these energies have a configuration of BAE roots where $\rho L - 2$ of them are real and symmetrically distributed around the origin, and the two out-most roots are in the form $\lambda = \pm(a + i\pi)$, with $a \in \Re$. There is a difficulty in using this set of eigenlevels. As we change the lattice size, their relative positions $m = m'$ in the conformal tower are not fixed. However, the estimates for the sound velocity obtained by direct diagonalization ($L \leqslant 24$) of the quantum chain, although with low precision, are enough to indicate the position $m = m'$ of the eigenlevel in the conformal tower. Using this procedure we computed the conformal anomaly at several points in regions 1 and 2 (see figure 1) obtaining $c = 1.00(1)$.

Since in regions 1 and 2 the ground state is described by real roots of the BAE, it is not difficult, in this case, to consider the bulk limit ($L \to \infty$) of the BAE (15)–(16). Following Baxter [15], we define the variables

$$x_j = \frac{Q_j}{L} = \frac{1}{2\pi}\left[k(\lambda_j) - \frac{1}{L}\sum_{l=1}^{\rho L}\theta(\lambda_j - \lambda_l)\right]. \tag{17}$$

When $L \to \infty$, $x_j \to x$ becomes a continuous variable in the interval $x_{\min} < x < x_{\max}$ satisfying the integral equation

$$x_j = \frac{Q_j}{L} = \frac{1}{2\pi}\left[k(\lambda_j) - \int_{x_{\min}}^{x_{\max}}\phi(\lambda(x) - \lambda(y))\,\mathrm{d}y\right]. \tag{18}$$

Since for the ground state the $\{Q_j\}$ are equally spaced by the unity, $\sigma_L(\lambda) = \frac{\mathrm{d}x}{\mathrm{d}\lambda}$ will give us, for $L \to \infty$, the local density of roots $\sigma_\infty(\lambda)$ that satisfies the integral equation

$$\sigma_\infty(\lambda) = \frac{1}{2\pi}\left(\frac{\mathrm{d}k(\lambda)}{\mathrm{d}\lambda} + \int_{-\lambda_0}^{\lambda_0}\frac{2\sqrt{3}\sigma_\infty(\lambda')}{2\cosh(2(\lambda-\lambda')) + 1}\,\mathrm{d}\lambda'\right), \tag{19}$$

where from (16)

$$\frac{\mathrm{d}k(\lambda)}{\mathrm{d}\lambda} = \frac{\sqrt{3}}{2\cosh(2\lambda)+1}\left(1 + \frac{\sqrt{3}\cosh\lambda}{\sqrt{\left(4t_p^2 - 1\right)\sinh^2\lambda + 3t_p^2}}\right), \tag{20}$$

and $\lambda_0 = \lambda_0(t_p, \rho)$ gives the extreme values of the roots. The total density of particles and the ground-state energy per site are given by

$$\rho = \int_{-\lambda_0}^{\lambda_0}\sigma_\infty(\lambda)\,\mathrm{d}\lambda, \tag{21}$$

$$\epsilon_0(t_p, \rho, h) = \epsilon_0(t_p, \rho, 0) - h\rho = -\rho\left(\frac{1}{2t_p} + h\right) + 2\int_{-\lambda_0}^{\lambda_0}\cos((k(\lambda))\sigma_\infty(\lambda)\,\mathrm{d}\lambda, \tag{22}$$

where $h = h(t_p, \rho)$ is the magnetic field that fixes the ground-state energy at the density ρ.

For $t_p < 1/2$ (region 1), $\lambda_0(t_p, \rho)$ is always finite, i.e. $\lambda_0(t_p, \rho, h) \leqslant \Omega(t_p)$ (see (14)). In figure 3 we show the ground-state energy $\epsilon_0(t_p, \rho, h)$ for several values of t_p in region 1 (we set $h = 0$ in the figure). They are obtained by using in (22) the $\sigma_\infty(\lambda)$ obtained from the numerical solution of the coupled integral equations (19)–(21). As we see from this figure these equations give us a maximum total density of particles $\rho = \rho_{\max}(t_p) < 1$ for the quantum chain. At the endpoints of the curves we have $\lambda_0 = \Omega(t_p)$ (see (14)). Above this density, which we refer as region 5, some of the BAE roots associated with the ground state of the quantum chain have complex values. In figure 1 the line separating regions 1 and 5 gives, for a given t_p, the maximum density obtained from (19) to (21). This line was obtained by solving numerically (19)–(21). In order to compare with the finite-size results, we give in the last line of table 1 the estimated value of $\epsilon_0(t_p, \rho, h = 0)$, obtained by solving (19)–(21) for $t_p = 0.2,\ 0.3$ and 0.4 with $\rho = 0.6,\ 0.65$ and 0.7, respectively.

For $t_p \geqslant 1/2$ (region 2), the roots $\{\lambda_j\}$ are not constrained and $\lambda_0 = \lambda_0(t_p, n)$ is arbitrary. The maximum density compatible with only real roots of the BAE for the ground state is obtained by setting $\lambda_0 \to \infty$ in (19) and (21). In this case we can solve (19)–(21) by using Fourier transforms. After some long but straightforward calculation, we obtain the maximum

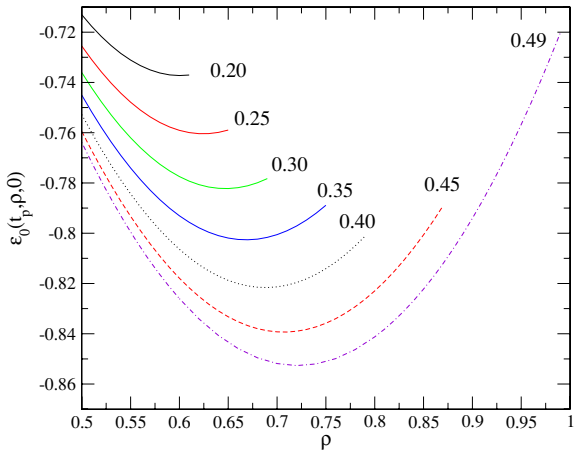

Figure 3. Ground-state energy per site of the Hamiltonian (1) as a function of the density ρ, for several values of t_p in region 1. In the figure we set $h = 0$ and the values of t_p are shown. These curves are obtained by solving (19)–(21). For a given value of t_p the curves are shown for $\rho < \rho_{\max}(t_p)$, with $\rho_{\max}(t_p)$ given by (23). For $\rho > \rho_{\max}(t_p)$ there exist complex roots in the BAE solutions for the ground state and the model is in region 5.

density

$$\rho_{\max}(t_p) = \int_0^\infty \frac{3\sqrt{3}}{2\cosh(2\lambda)+1}\left(1+\frac{\sqrt{3}\lambda}{\sqrt{\left(4t_p^2-1\right)\sinh^2\lambda+3t_p^2}}\right)\mathrm{d}\lambda. \tag{23}$$

At special values of t_p we are able to solve (23) analytically: $\rho_{\max}(1/2) = 1$, $\rho_{\max}(1) = 1/2$, $\rho_{\max}(\infty) = 1/4$. In figure 1 the curve separating region 2 from 3 was obtained from the numerical evaluation of (23). As occurred in region 5, for $\rho > \rho_{\max}(t_p)$ (regions 3 and 4), the BAE solutions giving the ground state contain complex roots besides the real ones.

As in region 1 (see table 1) we also calculated the finite-size corrections for the ground-state energy in several points of region 2. Using (11) and the same procedure as before our results indicate that, like region 1, region 2 is also critical and conformal invariant with $c = 1$. We then have in both regions (1 and 2) a massless behavior with ground-state energy given by real roots of the BAE. This critical behavior is quite similar to that of the XXZ quantum chain in the presence of a magnetic field [16, 17]. We then expect in regions 1 and 2 a physical behavior described by an underlying $c = 1$ Coulomb gas conformal field theory. The anomalous dimensions of operators are given by

$$x_{l,m} = l^2 x_p + m^2/4x_p, \tag{24}$$

with $l, m = 0, \pm1, \pm2, \ldots$. The dimensions $l^2 x_p$ are obtained from (12), by considering the difference between the ground-state energies in the sectors with densities ρ and $\rho + l/L$. The dimensions $x_{0,m}$ are calculated by using in (12) the mass gaps associated with eigenstates with the same density of particles.

The parameter $x_p = x_p(t_p, \rho)$ in regions 1 and 2, which are estimated from the finite-size corrections of the energy (22), can be calculated analytically. This is done by applying to our relations (18)–(22) the method used in [16] for the XXZ quantum chain in a magnetic field. We obtain

$$x_p = (2\xi(\lambda_0))^{-2}, \tag{25}$$

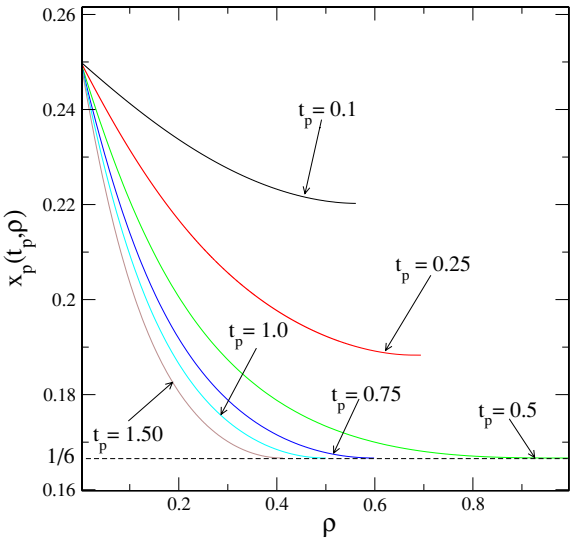

Figure 4. The values of $x_p(t_p, \rho)$ (see (24)) as a function of ρ for several values of t_p in regions 1 and 2. The curves with $t_p < 1/2$ and $t_p \geqslant 1/2$ belong to regions 1 and 2 of figure 1, respectively. The endpoints of the curves are the densities separating regions 1 and 2 from 3 and 5, respectively. For $t_p \geqslant 1/2$ the endpoints of the curves are $x_p = 1/6 \sim 0.166\,66$.

where $\xi(\lambda_0)$ is the dressed charge [18] evaluated at the Fermi surface λ_0 of the effective Coulomb gas. This function satisfies the integral equation

$$\xi(\lambda) = 1 + \frac{\sqrt{3}}{\pi} \int_{-\lambda_0}^{\lambda_0} \frac{\xi(\lambda')}{2\cosh(\lambda - \lambda') + 1}\, \mathrm{d}\lambda'. \tag{26}$$

In figure 4 we show, for several values of t_p in regions 1 and 2, the dimensions $x_p = x_p(t_p, \rho)$ obtained by using in (25) the numerical solutions of the coupled integral equations (19), (21) and (26). We can see from this figure that for any t_p, as $\rho \to 0$, $x_p \to 1/4$. This can be understood from the fact that at this limit the interacting potential energy is negligible when compared with the kinetic energy (hopping terms). We have essentially non-interacting particles, where x_p has the value 1/4. We also see from this figure that for $t_p < 1/2$ (region 1), the limiting value of x_p depends on the value of t_p. This value is obtained by choosing $\lambda_0 = \Omega(t_p)$ in (26), where $\Omega(t_p)$ is given by (14). In figure 5 we show the limiting values of x_p as a function of t_p for $t_p \leqslant 1/2$. It varies from $x_p = 1/4$ to $x_p = 1/6$ as t_p goes from 0 to 1/2. Moreover, figure 4 shows that the limiting value is $x_p = 1/6$ for any $t_p \geqslant 1/2$. This should be the case since for any $t_p \geqslant 1/2$ the maximum value of λ_0 is infinity and consequently (25) and (26) give us the same result for any value of t_p. The exact value $x_p = 1/6$ can be understood from the relation (see section 2) of the model at $t_p = 1$ and the XXZ chain with anisotropy $\Delta = 1/2$. When $\lambda_0 \to \infty$ the density $\rho \to 1/2$. At this density the XXZ has no magnetic field and its exponent is given by $x_p = (\pi - \cos^{-1}(-\Delta))/2\pi = 1/6$. These results imply that, at the line separating regions 1 and 5, x_p varies continuously from 1/4 to 1/6 and, in the line separating regions 2 and 3, it remains fixed to the value 1/6.

In regions 3 and 5 of figure 1 some of the roots of the BAE corresponding to the ground state have complex values. In fact in some points of these regions we were able, for small lattice sizes, to solve the BAE for the ground-state energy. We verified that besides real roots we also have pairs of 2-strings (pair of roots of type $\lambda_\pm = a + \mathrm{i}b$, with $a, b \in \Re$). The simultaneous appearance of complex roots in the BAE (8) produces numerical instabilities

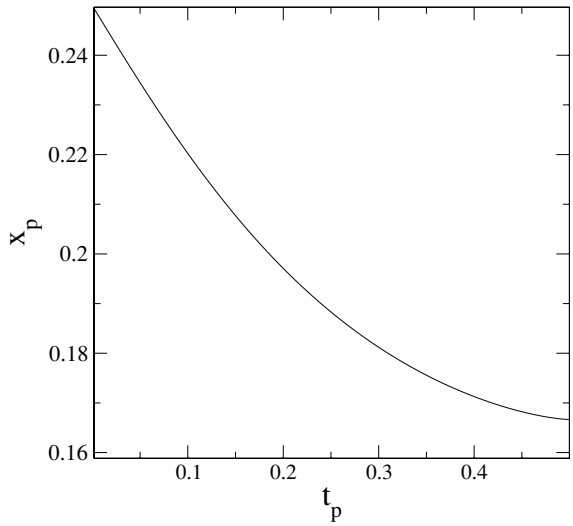

Figure 5. The values of x_p at the line separating regions 1 and 5 (see figure 1). The exponents varies from $x_p = 1/4$ to $x_p = 1/6 \sim 0.1666$, as t_p goes from 0 to $1/2$.

Table 2. The quantities $e_\infty, v_s, c, x_{+1,0}, x_{-1,0}$ and $x_{0,1}$ for the Hamiltonian (1) with density $\rho = 1/2$ and some values of t_p. The first line ($t_p = 0.75$) corresponds to a point inside region 2 and the second one ($t_p = 1$) to a point at the line separating regions 2 and 3. The remaining lines correspond to points in region 3 (see figure 1).

t_p	e_∞	v_s	h	c	$x_{+1,0}$	$x_{-1,0}$	$x_{0,1}$	$1/4x_{0,1}$
0.75	−1.119 47	1.4321	−1.5911	1.000	0.168	0.169	1.490	0.168
1.0	−1.049 04	1.2991	−1.5000	0.999	0.167	0.167	1.500	0.167
1.15	−1.022 11	1.2252	−1.4686	0.999	0.170	0.169	1.498	0.167
1.25	−1.007 92	1.1771	−1.4540	1.001	0.169	0.167	1.490	0.168
1.35	−0.995 97	1.1300	−1.4425	1.001	0.169	0.167	1.490	0.168
1.50	−0.9812	1.0596	−1.4295	1.01	0.169	0.167	1.48	0.168

causing the numerical solution of the BAE to become quite difficult task. Due to this difficulty, instead of solving the BAE (8) we have used the power method to calculate the lower part of the eigenspectrum. In this case, due to computer limitations, even exploring the $U(1)$ and translation symmetries of the quantum chain, we are restricted to lattice sizes up to $L = 24$, where the largest sector we can calculate the lowest eigenenergy has dimension 5136 935 ($L = 24$, $n = 13$). Since we work at a fixed density of particles, the larger number of sites we can use (and consequently obtain a better precision for our estimates) is at the density $\rho = 1/2$.

In table 2 we present some of our estimated values of several quantities that characterize the critical behavior of the quantum chain (1) inside region 3 ($t_p = 1.15$, 1.15, 1.35 and 1.5). The calculations were done at density $\rho = 1/2$. In the first two lines, for comparison, we also give the results for a point inside region 2 ($t_p = 0.75$) and a point at the line separating regions 2 and 3 ($t_p = 1$). We include in the table the estimated values for the ground-state energy per particle in the bulk limit e_∞ (we set $h = 0$ in (1)), the sound velocity v_s and the magnetic field h that fixes the ground state at density $\rho = 1/2$.

The value of the exponent $x_{+1,0} = x_{-1,0} = x_p$ for $t_p = 0.75$ and $t_p = 1$ is known from the solutions of (19), (21) and (26), i.e. $x_p = 0.167\,70$ ($t_p = 0.75$) and $x_p = 0.1666$ ($t_p = 1$). The

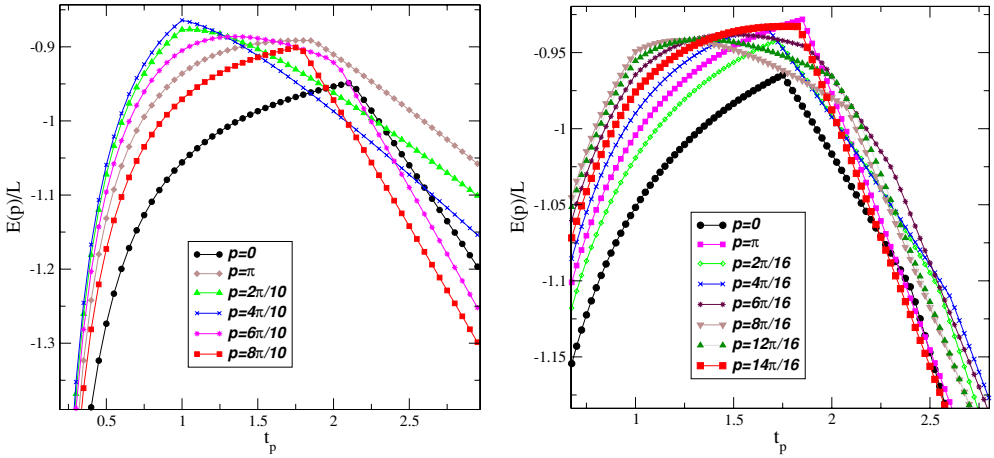

Figure 6. Lowest eigenenergy $E(p)$ with momentum p, as a function of t_p for the Hamiltonian (1) at density $\rho = 1/2$ and lattice sizes $L = 10$ (left) and $L = 16$ (right). We set $h = 0$ in the figure. The energies $E(p)$ are the lowest eigenenergies with momentum p. The eigenlevels with $p \neq 0, \pi$ are doubled degenerated (momenta p and $-p$). The kinks on the curves are due to a level crossing among the two lowest eigenenergies with the same momentum.

comparison of these last results with the first two lines of table 2 indicates that the errors are in the last digit. Like regions 1 and 2, region 3 is also massless with a conformal central charge $c = 1$. The dimensions $x_{+1,0}$ and $x_{-1,0}$ in table 2 are associated with the sectors with densities $\rho = \frac{1}{2} + \frac{1}{L}$ and $\rho = \frac{1}{2} - \frac{1}{L}$, respectively. These dimensions in a standard Coulomb gas phase, like in regions 1 and 2, are equal and correspond to the dimensions $x_{\pm 1,0}$ in (24). We also show in table 2 the dimension $x_{0,1}$ related to the first gap with zero (mod. π) momentum in the sector containing the ground state. The dimensions $x_{\pm 1,0}$, as shown in the table, is close to $1/4x_{0,1}$, in agreement with (24). The dimensions in the first two lines of table 2 ($t_p = 0.75$ and $t_p = 1$) although close are not equal, as we can also check in figure 4. Table 2 also indicates that inside region 3 the conformal dimensions almost do not change as we change t_p. Since our results are valid only for the density $\rho = 1/2$ we do not know if this small (or no) variation remains valid for other points inside region 3.

Once in region 3 of figure 1 by increasing the value of t_p, for a fixed density, we reach region 4. In this region several eigenlevels' crossings occur in the finite lattice. In figure 6 we show for $L = 10$ (left) and $L = 16$ (right) these crossings. The crossings among eigenlevels with distinct momenta are visualized directly in the figure. The kinks in the curves are due to the level crossings with the same momentum.

As we cross from region 3 to region 4, the ground-state energy shows a discontinuity on its derivative due to a change of its relative position with an excited eigenstate. Unfortunately also in this region, due to numerical instabilities, it is quite difficult to solve directly the BAE (8). The direct diagonalization of the quantum chain, except at the density $\rho = 1/2$, can only be done for quite few lattice sizes. Our estimate of the line separating regions 3 and 4, shown in figure 1, is then just schematic. This indicates a first-order phase transition along the line separating these regions.

Inside region 4 and for $\rho = 1/2$, we verify that the leading finite-size correction of the ground-state energy is not $O(1/L^2)$ as expected in a massless conformaly invariant phase (see (11)). This is illustrated in figure 7 where we show for some values of t_p the ground-state energy as a function of $1/L^2$ for the density $\rho = 1/2$. We see in this figure the distinct behavior for the points belonging to regions 2 and 3 as compared with those of region 4 (lower two

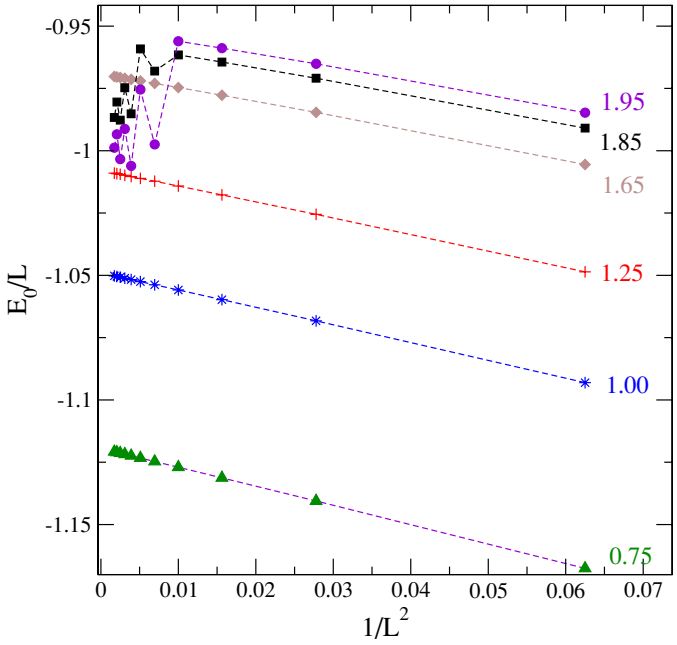

Figure 7. Ground-state energy per particle as a function of L^{-2} for the Hamiltonian (1) with $h = 0$ at density $\rho = 1/2$. The lattice sizes are $L = 6, 8, \ldots, 24$. The curves correspond to $t_p = 0.25, 0.5$ (region 1), $t_p = 0.75, 1.00$ (region 2), $t_p = 1.25$ (region 3) and $tp = 1.85, 1.95$ (region 4).

curves). The oscillatory behavior in figure 7 for the points inside region 4 is a consequence of the level crossings occurring inside this region. As we can see in figure 6 for $t_p \sim 1.65$ many crossings occur with the crossing position dependent of the lattice size. As we change t_p inside this region, for a given finite lattice L, the momentum of the ground state also changes. For example for $t_p \approx 2.25$ (see figure 6) the ground state for the quantum chains with $L = 10$ and $L = 16$ has a nonzero momentum and is doubled degenerated. The oscillatory behavior shown in figure 7 turns out the finite-size scaling analysis quite imprecise. Although not conclusive these oscillatory behavior in energy and momentum indicates that we have in region 4 effects of incommensurability of the density distributions, similar to that occurring in other models [19].

In region 5, as in region 3, it is difficult to solve numerically the BAE due to the occurrence of complex roots mixed with the real ones. In this case our analysis was restricted to small lattice sizes ($L \leqslant 24$). Since we should consider a sequence of lattices with fixed density and on this region $\rho > 1/2$, the number of data we can have on a given finite-size sequence is quite small. However, for a given lattice size and density, as we change t_p we did not see the crossings of eigenlevels observed in region 4 (see figure 6). This indicates that region 5, similarly as regions 1, 2 and 3, is a critical $c = 1$ Coulomb gas phase. We greatly welcome more precise and convincing results for regions 4 and 5.

4. Summary and conclusions

We have made a detailed analysis of the spectral properties and phase diagram of one of the new spin-1 models introduced in [6]. This model is exactly integrable for arbitrary values

of the parameter t_p. Our analysis was restricted to the cases where $t_p > 0$. At $t_p = 1$ we have shown that the model recovers the deformed $SU(3)$ Perk–Schultz model (or the spin-1 Sutherland model) at the special value of its deformation parameter $q = e^{i2\pi/3}$ and external magnetic field. We verified that at this point the low-lying eigenvalues of the model are the same as the corresponding ones of the XXZ quantum chain with anisotropy $\Delta = 1/2$. We can then interpret the model we studied as an integrable generalization of the deformed $SU(3)$ Perk–Schultz model or the XXZ quantum chain at anisotropy $\Delta = -(q+1/q)$ with $q = e^{i2\pi/3}$.

The BAE, whose solutions give the eigenspectrum of the model, are quite difficult to solve analytically or numerically for general values of the parameter t_p and density of particles (magnetization). Our results are summarized in figure 1, where we have regions 1–5.

Regions 1, 2, 3 and 5 belong to a critical phase governed by an underlying Coulomb gas conformal field theory with critical exponents varying continuously. We distinguished these regions according to the BAE roots of the low-lying eigenenergies of the quantum chain. In regions 1 and 2 these roots are real. This fact allowed us to solve directly the BAE for quite large lattices ($L \sim 1000$). Exploring conformal invariance we obtain good estimates for the conformal anomaly and anomalous dimensions of operators of the underlying conformal field theory. In these two regions we could take the thermodynamic limit and obtain the critical exponents in terms of integral equations (see (25)–(26)).

In regions 3, 4 and 5 the BAE roots corresponding to the ground state are not real and very difficult to calculate even for relatively small lattice sites. In these regions our analyses were based on the direct calculation of the eigenspectra for lattices sizes $L \leqslant 24$.

Our results indicated that regions 3 and 5, although having BAE complex roots in the ground state, have the same critical behavior as in regions 1 and 2. Actually regions 1, 2, 3 and 5 are quite similar to the XXZ quantum chain in the presence of a magnetic field, with anomalous dimensions $x_{l,m}$ given by (24), with the value of x_p depending on t_p and ρ.

As we cross from region 3 to region 4, there is a discontinuity of the ground-state energy. This is due to a crossing of the two lowest eigenenergies, and we expect that regions 3 and 4 are separated by a first-order phase transition.

Inside region 4 we found an oscillatory behavior for the energy gaps and momentum of the ground state, as we change the lattice size or the anisotropy parameter t_p. These oscillations are due to a large number of crossing of eigenlevels. These crossings made our finite-size analysis imprecise. We believe that probably such oscillatory behavior is due to incommensurability effects on the charge (local magnetization) distribution in the lattice, as occurs in other models whose incommensurability is established [19].

We conclude mentioning two interesting open problems for the future: the derivation of the R-matrix associated with this new integrable spin-1 model and the extension of the present study to the second exactly integrable model introduced in [6]. This second model at $t_p = 1$ is related to the XXZ quantum chain with anisotropy $\Delta = -1/2$. This last model has remarkable properties. It is related to the problem of enumerating alternated sign matrices [20] and the Hamiltonian with open boundaries is the evolution operator of a conformal invariant stochastic model, namely the raise and peel model [21]. We then expect that the second model in [6] with values of $t_p \neq 1$ may also have interesting connections with other interesting problems in physics and combinatorics.

Acknowledgments

We thank V Rittenberg for discussions and a careful reading of the manuscript. This work has been partially supported by the Brazilian agencies FAPESP and CNPq.

References

[1] Yang C N and Yang C P 1966 *Phys. Rev.* **150** 321
Yang C N and Yang C P 1966 *Phys. Rev.* **150** 327
[2] Zamolodchikov A B and Fateev V 1980 *Sov. J. Nucl. Phys.* **32** 298
Babujian H 1982 *Phys. Lett.* **90A** 479
Alcaraz F C and Martins M J 1988 *Phys. Rev. Lett.* **61** 1529
[3] Izergin A G and Korepin V E 1981 *Commun. Math. Phys.* **79** 303
[4] Virchirko V I and Reshetikhin N Yu 1983 *Theor. Math. Phys.* **56** 805
[5] Parkinson J B 1987 *J. Phys. C: Solid State Phys.* **20** L1029
Klümper A 1989 *Europhys. Lett.* **9** 815
Batchelor M T, Mezincescu L, Nepomechie R I and Rittenberg V 1990 *J. Phys. A: Math. Gen.* **23** L141
Alcaraz F C and Malvezzi A L 1992 *J. Phys. A: Math. Gen.* **25** 4535
Köberle R and Santos A L 1994 *J. Phys. A: Math. Gen.* **27** 5409
[6] Alcaraz F C and Bariev R Z 2001 *J. Phys. A: Math. Gen.* **34** Ll467
[7] Alcaraz F C and Lazo M J 2004 *J. Phys. A: Math. Gen.* **37** L1
Alcaraz F C and Lazo M J 2004 *J. Phys. A: Math. Gen.* **37** 4149
[8] Blume M 1966 *Phys. Rev.* **141** 517
Capel H W 1966 *Physica (Amsterdam)* **32** 966
Alcaraz F C, Drugowich de Felício J R, Köberle R and Stilck J F 1985 *Phys. Rev.* B **32** 7469
Haldane F D M 1983 *Phys. Rev. Lett.* **50** 1153
Alcaraz F C and Hatsugai Y 1992 *Phys. Rev.* B **46** 13914
[9] Kulish P P and Sklyanin E K 1981 *Lecture Notes Phys.* **151** 61
[10] Perk J H H and Schultz C L 1981 *Phys. Lett.* A **84** 407
Schultz C L 1983 *Physica* A **122** 71
[11] Sutherland B 1975 *Phys. Rev.* B **12** 3795
[12] Alcaraz F C and Stroganov Yu G 2002 *J. Phys. A: Math. Gen.* **35** 3805
Alcaraz F C and Stoganov Yu G 2003 *J. Phys. A: Math. Gen.* **36** 2381
[13] Blöte H W J, Cardy J L and Nightingale M P 1986 *Phys. Rev. Lett.* **56** 742
Affleck I 1986 *Phys. Rev. Lett.* **56** 746
[14] Cardy J L 1987 *Phase Transitions and Critical Phenomena* vol 11, ed C Domb and J L Lebowitz (New York: Academic) p 55
Cardy J L 1986 *Nucl. Phys.* B **270** 186
[15] R J Baxter R J 1982 *Exactly Solved Models in Statistical Mechanics* (New York: Academic)
[16] Woynarovich F, Eckle H P and Truong T T 1989 *J. Phys. A: Math. Gen* **22** 4027
[17] Jonhson J D and McCoy B M 1972 *Phys. Rev.* A **6** 1613
Takanishi 1973 *Prog. Theor. Phys.* **50** 1519
Alcaraz F C and Malvezzi A L 1995 *J. Phys. A: Math. Gen.* **28** 1521
[18] Korepin V E 1979 *Teor. Math. Fiz.* **41** 169
[19] Aligia A A, Batista C D and Essler F H L 2000 *Phys. Rev.* B **62** 3259
Hoeger C, von Gehlen G and Rittenberg V 1985 *J. Phys. A: Math. Gen.* **18** 1813
[20] Razumov A V and Stroganov Yu G 2001 *J. Phys. A: Math. Gen.* **34** 3185
Batchelor M T, de Gier J and Nienhuis B 2001 *J. Phys. A: Math. Gen.* **34** L265
Razumov A V and Stroganov Yu G 2001 *J. Phys. A: Math. Gen.* **34** 5335
de Gier J, Batchelor M T, Nienhuis B and Mitra S 2001 *J. Math. Phys.* **43** 4235
[21] de Gier J, Nienhuis B, Pearce P A and Rittenberg V 2204 *J. Stat. Phys.* **114** 1
Alcaraz F C and Rittenberg V 2007 *J. Stat. Mech.* P07009